### Proximal Causal Inference for Modified Treatment Policies

## Antonio Olivas-Martinez<sup>1,\*</sup>, Peter Gilbert<sup>1,2,3</sup>, and Andrea Rotnitzky<sup>1</sup>

<sup>1</sup>Department of Biostatistics, University of Washington, Seattle, WA, U.S.A.
 <sup>2</sup>Vaccine and Infectious Disease Division, Fred Hutchinson Cancer Center, Seattle, WA, U.S.A.
 <sup>3</sup>Public Health Science Division, Fred Hutchinson Cancer Center, Seattle, WA, U.S.A.
 \*email: aolivas@uw.edu

Summary: The proximal causal inference framework has advanced the identification and inference of causal effects in scenarios involving unobserved confounding and two disjoint sets of observed strong proxies for the unmeasured confounders—commonly referred to as negative control treatments and negative control outcomes. Proximal causal inference has predominantly been explored for target estimands that contrast counterfactual worlds, where subjects follow specific pre-specified treatment regimes, which may be randomized and could depend on observed covariates. However, when dealing with continuous exposures, a compelling alternative estimand exists—the mean under a modified treatment regime. This concept envisions a world in which each individual receives a treatment dose corresponding to their actual dose but modified in a pre-specified manner. In this work, we extend the proximal causal inference framework to encompass the identification and estimation of the mean of an outcome under a modified treatment regime, specifically for a continuous point-exposure, bridging an important gap in the literature. Our approach leverages modern debiased machine learning techniques, using non-parametric estimators of nuisance functions to avoid restrictive parametric assumptions, thereby enabling inference across a broad range of datagenerating processes. We illustrate our proposal by applying it to immunobridging trials of COVID-19 vaccines, focusing on identifying correlates of protection. This extension broadens the applicability of proximal causal inference, providing valuable insights into the estimation of treatment effects in scenarios involving continuous exposures. KEY WORDS: Proximal causal inference, modified treatment policy, unmeasured confounding, double robustness, observational study, stochastic intervention

### 1. Introduction

Vaccines are crucial for public health, but their development requires a rigorous assessment, including phase 3 efficacy studies. While these trials are indispensable, they often require lengthy follow-up periods and raise ethical concerns about the use of placebos, particularly when vaccines have already proven effective in other populations. To address these challenges, researchers seek to identify early vaccine-induced immune markers that predict later outcomes, known as correlates of protection (Plotkin, 2010; Fleming and Powers, 2012). These correlates can serve as surrogates in future studies, potentially expediting vaccine development and approval processes while maintaining safety and efficacy standards.

Identifying correlates of protection involves characterizing the causal effect of a continuous exposure (the immune marker) on the outcome of interest. A natural approach to assessing this effect is through the causal dose-response curve, which summarizes the expected outcome as a function of the immune marker level. Using the potential outcomes framework, this model envisions a hypothetical world where the vaccine induces a particular immune marker level in all individuals, with the summary of interest corresponding to the mean outcome in that counterfactual scenario.

An alternative approach, that has gained popularity in recent years, is to consider a counterfactual world where individuals receive a modified treatment policy (MTP) (Robins, 1986; Diaz Munoz and van der Laan, 2012; Haneuse and Rotnitzky, 2013). An MTP is an intervention that assigns each individual a treatment dose corresponding to their observed dose in the trial, but modified in a pre-specified manner. The counterfactual MTP mean provides a method to evaluate how the overall vaccine efficacy would change under under pre-specified shifts in the vaccine-induced immune marker levels (the correlate of protection) from their observed values (Hejazi et al., 2021; Huang et al., 2023). These shift interventions are more realistic because they envision a world where the vaccine induces in everyone

an immune marker dose shifted by a pre-specified amount from their observed dose, which could potentially be achieved with a different vaccine formulation. Importantly, the treatment assignment under an MTP can also depend on baseline covariates, allowing for more flexible and realistic interventions. For instance, the treatment shift could vary based on factors such as age, immunocompetency status, or other individual characteristics.

An additional complication when assessing immune markers as correlates of protection is that vaccine-induced immune marker levels cannot be randomized, making this analysis susceptible to confounding. In particular, an individual's underlying immunity level is likely a strong unobserved confounder. A promising solution to this challenge is the proximal causal inference framework, recently introduced by Miao, Geng, and Tchetgen Tchetgen (2018); Tchetgen Tchetgen et al. (2020); and Cui et al. (2023). This framework enables the identification and inference of causal effects in scenarios involving unobserved confounding, provided we have access to two disjoint sets of observed strong proxies for the unmeasured confounders. These proxies are commonly referred to as negative control treatments and negative control outcomes. Negative control treatments are variables that lack a direct impact on the outcome of interest, while negative control outcomes are variables that remain unaffected by both the negative control treatments and the primary treatment of interest. Figure 1 provides a visual representation of a causal diagram incorporating these negative control variables, illustrating their relationships within the framework. The proximal causal inference framework is well-suited for identifying correlates of protection in vaccine efficacy studies, as these trials routinely measure variables that qualify as negative controls, making the framework's application both feasible and relevant. While estimators of the counterfactual MTP mean under the assumption of no unmeasured confounders have been extensively studied (Diaz Munoz et al., 2012; Haneuse et al., 2013; Hejazi et al., 2021), to our knowledge, estimators under the proximal causal inference assumptions have not yet been developed for this context. In this paper, we address this gap by proposing a novel estimator of the counterfactual MTP mean that leverages the proximal causal inference framework to assess immune markers as correlates of protection in vaccine efficacy studies.

In Section 2, we present our motivating example, the ENSEMBLE trial, highlighting the proxies used to address unmeasured confounding. Section 3 introduces the causal estimand of interest and the assumptions that allow for its identification. In Section 4, we describe our estimator and provide its asymptotic analysis. Section 5 evaluates the finite sample properties of our estimator through numerical experiments. In Section 6, we apply our estimator to identify correlates of protection in the ENSEMBLE trial. Finally, we offer general conclusions and future research directions in Section 7.

## [Figure 1 about here.]

## 2. Motivating example

We aim to investigate vaccine-induced neutralizing antibody levels at day 29 (D29) post-vaccination as correlates of protection against symptomatic COVID-19 infection in the first 7 months post antibody measurement. This immune marker has been identified as a correlate of protection across various vaccine platforms through multiple research approaches (Gilbert et al., 2022a,b; Fong et al., 2022, 2023; Feng et al., 2021). Our analysis utilizes data from the ENSEMBLE trial, a multinational, randomized, placebo-controlled phase 3 study assessing the efficacy of a single dose of Ad26.COV2.S in preventing symptomatic SARS-CoV-2 infection (Sadoff et al., 2022).

Potential observed confounders include age, participant's region of residence, and a predefined risk score for acquiring symptomatic COVID-19 infection, while an individual's immunity level is likely a strong unmeasured confounder. The ENSEMBLE trial measured strong proxies of the immune system level that can serve as negative controls: anti-spike binding antibody levels at D29 as negative control treatments and the burden of respiratory symptoms unrelated to SARS-CoV-2 infection during trial follow-up as negative control outcomes.

Measuring anti-spike binding antibodies is a more accessible alternative to assessing neutralizing antibodies, as it does not require biosafety level 2 or 3 facilities. However, the anti-spike binding antibody assay has a key limitation: it only detects antibodies that bind to the SARS-CoV-2 spike protein without distinguishing those with actual neutralizing activity. Thus, while it can identify the presence of antibodies, it cannot measure their capacity to neutralize the virus (Sholukh et al., 2022). In our analysis, we treat anti-spike binding antibodies as suitable negative control treatments. This approach aligns with an immunological model where binding to the spike protein is a necessary intermediate step in antibody-mediated protection, but only neutralizing antibodies directly block host cell infection. Under this model, anti-spike binding antibodies should not have an independent effect on the outcome once neutralizing antibodies are accounted for.

Similarly, SARS-CoV-2-specific antibodies should not protect against other respiratory infections, making non-COVID respiratory symptoms suitable negative control outcomes. The burden of these symptoms serves as a proxy for an individual's general susceptibility to respiratory infections, which may correlate with their underlying immunity level without being directly affected by SARS-CoV-2 antibodies.

It is essential to acknowledge that our knowledge of immune responses to SARS-CoV-2 is rapidly advancing. Ongoing research will likely enhance our understanding of these immunological dynamics and the specific functions of various antibody types.

### 3. Target of Inference and Identification

Consider an observational study comprising n individuals randomly selected from a target population. For each subject i = 1, ..., n, we observe a continuous exposure  $X_i$ , an outcome

 $Y_i$ , and m potential confounders  $L_i = (L_{i,1}, \ldots, L_{i,m})$ . Let  $Y_i(x)$  be the counterfactual outcome when subject i receives exposure level  $X_i = x$ . For any random vector V, let  $\sup V$  denotes its support. We are interested in estimating

$$\psi_0 = \mathbb{E}\left[Y_i\left\{q(X_i, L_i)\right\}\right],\,$$

where  $q: \operatorname{supp}(X, L) \to \mathbb{R}$  is a given function. For instance, if  $q(x, l) = x + \delta$ , then  $\psi_0$  is the expected value of the outcome in a hypothetical scenario where every subject receives an exposure that is  $\delta$  units higher than the exposure they actually received.

In our motivating example, our sample consists of the participants randomized to the vaccine arm in the ENSEMBLE trial who actually received the vaccine and were sero-negative at enrollment (i.e., had no detectable levels of antibodies against the SARS-CoV-2 virus). Here, X represents vaccine-induced neutralizing antibody levels at D29 on a base 10 logarithmic scale, Y indicates symptomatic COVID-19 infection between 7 and 210 days post-D29, and L includes potential confounders as described earlier. In this case, when  $q(x, l) = x + \delta$ ,  $\psi_0$  corresponds to the probability of symptomatic COVID-19 in a hypothetical world where each participant's neutralizing antibody levels are  $10^{\delta}$  times higher than observed in the trial.

To identify correlates of protection, we aim to evaluate the effects of increasing everyone's neutralizing antibody levels by  $\delta$  units on a log-10 scale. However, this approach is unfeasible because, for each observed antibody level x, we would need a corresponding participant with a level of  $x + \delta$  and identical confounders. The outcome of this second participant would represent the hypothetical outcome of the first if they had developed  $\delta$  units more neutralizing antibodies. In practice, this is unfeasible because it would require the support of X given L to be unbounded. To address this issue, two strategies can be employed. One strategy is to restrict the population over which we compute  $\mathbb{E}\left[Y\left\{q(X,L)\right\}\right]$ . Another strategy is to

change the policy q(x, l) so that its image always lies within the support of X. We elaborate on these strategies in the following examples.

EXAMPLE 1 (First strategy: Restricting the population): Assuming the existence of functions  $c: \operatorname{supp}(L) \to \mathbb{R}$  and  $d: \operatorname{supp}(L) \to \mathbb{R}$  satisfying for each  $l \in \operatorname{supp}(L)$ ,  $c(l) < d(l) - \delta$  and  $[c(l), d(l)] \equiv \operatorname{supp}(X|L=l)$ , we change the target parameter to  $\mathbb{E}\left\{Y(X+\delta)|(X,L) \in \mathcal{S}\right\}$  where  $\mathcal{S}:=\{(x,l): l \in \operatorname{supp}(L), x \in [c(l), d(l) - \delta]\}$ .

EXAMPLE 2 (Second strategy: Changing the target policy): We change the target parameter to  $\mathbb{E}\left[Y\left\{q^{\epsilon}(X,L)\right\}\right]$  where  $\varepsilon$ :  $\mathrm{supp}(L) \to (0,\infty)$  is a function such that for every  $l \in \mathrm{supp}(L)$ ,  $c(l) < d(l) - \delta - \varepsilon(l)$ , and

$$q^{\varepsilon}(x,l) = \begin{cases} x + \delta & \text{if } x \in [c(l), d(l) - \delta - \varepsilon(l)), \\ x + \frac{\delta}{\delta + \varepsilon(l)} \left\{ d(l) - x \right\} & \text{if } x \in [d(l) - \delta - \varepsilon(l), d(l)]. \end{cases}$$
 (1)

Within the stratum L = l, this policy shifts each individual's observed exposure value by  $\delta$  if the observed value is lower than  $d(l) - \delta - \varepsilon(l)$ , or by  $\frac{\delta}{\delta + \varepsilon(l)} \{d(l) - x\}$  otherwise. Notably, for individuals with an observed exposure value within  $\delta + \varepsilon(l)$  units from d(l), the shift decreases in proportion to the exposure value. For individuals with an observed exposure value of d(l), the policy makes no shift.

The shift intervention introduced in Example 1 is an ideal intervention of interest; but the counterfactual mean under this shift intervention is restricted to a subset of the target population. In contrast, the counterfactual mean under the alternative policy presented in Example 2 is over the entire population and differs from the ideal one in that subjects with observed exposures slightly smaller to the largest observable X given L = l are shifted by decreasingly smaller shifts.

We will discuss estimation of  $\psi_0$  for policies q that, like the policy in Example 2, can be implemented in the entire population, that is, q(x, l) belongs to  $[c(l), d(l)] \equiv \text{supp}(X|L=l)$ 

for all  $(x, l) \in \text{supp}(X, L)$ . In the Web appendix A, we provide the extension of our methodology to estimate the counterfactual mean in a restricted population.

### 3.1 Proximal Identifying Assumptions

Even for policies whose range falls within the support of X, the counterfactual MTP mean  $\psi_0$  cannot be identified in vaccines studies due to the unobserved individual immune status, which is a critical confounder. Building on the remarkable work of Miao et al. (2018); Tchetgen Tchetgen et al. (2020); Cui et al. (2023) (see also Kallus et al. (2022)), we show that  $\psi_0$  becomes identifiable if, in addition to baseline covariates L, we measure a negative control treatment Z and a negative control outcome W. Heuristically, after accounting for the observed confounders L, a negative control treatment Z is a potential cause of the exposure X that can only influence the outcome Y through the exposure X. Additionally, Z is influenced by the unmeasured confounder U. Similarly, a negative control outcome W potentially affects Y and is influenced by the unmeasured confounder U, but it is unaffected by the treatment X and the negative control treatment Z. These relationships are illustrated in Figure 1.

Specifically, we assume that  $(U_i, L_i, Z_i, W_i, X_i, Y_i)$  are n i.i.d. copies of a random vector (U, L, Z, W, X, Y), and for each subject i, we observe  $O_i = (L_i, Z_i, W_i, X_i, Y_i)$  but never observe  $U_i$ . We proceed under the following assumptions:

Assumption 1 (Consistency): Y(X) = Y.

Assumption 2 (Randomization of policy related populations): For all  $(x, l, u) \in \text{supp}(X, L, U)$  and x' = q(x, l), it hols that law  $\{Y(x')|X = x, L = l, U = u\} = \text{law}\{Y(x')|X = x', L = l, U = u\}$ 

Assumption 3 (Common support): For all  $(l, u) \in \text{supp}(L, U)$ , supp  $(X|L = l, U = u) \equiv \text{supp}(X|L = l)$ .

Assumption 4 (Negative control treatment):  $Z \perp Y \mid X, L, U$ .

Assumption 5 (Negative control outcome):  $(X, Z) \perp W \mid U, L$ .

The first assumption is standard in causal inference. The second assumption, introduced by Haneuse and Rotnitzky (2013), is specific to MTPs, and only requires conditional randomization between the observed values and those enforced by the policy. This is weaker than a conditional randomization assumption that assumes that every individual can receive any exposure level. Assumption 3 is standard in proximal causal inference and cannot be refuted because U is unobserved. It is the analogue to the positivity assumption of the propensity score in the literature on proximal inference, which also involves positivity conditional on the unmeasured confounders (Miao et al., 2018; Tchetgen Tchetgen et al., 2020; Kallus et al., 2022; Ghassami et al., 2022; Cui et al., 2023).

Assumptions 4 and 5 formalize the negative control relationships depicted in Figure 1. In our motivating example, anti-spike binding antibodies act as negative control treatments within an immunological framework where they influence the outcome solely through their neutralizing activity. Meanwhile, the burden of non-COVID-19 respiratory symptoms serves as a negative control outcome, as these symptoms should not be affected by SARS-CoV-2 antibodies.

We also impose the following assumption on the MTP:

Assumption 6 (Monotone and smooth policy): For each  $l \in \text{supp}(L)$ ,  $q(\cdot, l)$  is strictly monotone and differentiable almost everywhere with respect to the distribution of X given L = l.

This assumption ensures that for each l, the policy map  $q: x \mapsto q(x, l)$  has an inverse that is almost everywhere differentiable with respect to the distribution of X given L = l. This enables us to use data from study participants with L = l and exposure X = x, to infer

the counterfactual MTP outcome distribution for participants with exposure value in the actual study equal to  $q^{-1}(x, l)$ . Both the shift intervention policy and its modified version, as discussed in Example 2, satisfy this assumption.

Lastly, we require the following two assumptions which enable us to leverage negative controls for mitigating unobserved confounding. For any random vector V, hereafter,  $\mathcal{L}^2(V)$  denotes the space of functions of V with finite second moment.

Assumption 7 (Outcome bridge): There exists  $h_0 \in \mathcal{L}^2(X, L, W)$  solving for all  $(x, l, u) \in \text{supp}(X, L, U)$ , the integral equation

$$\mathbb{E}(Y|X = x, L = l, U = u) = \int h(x, l, w) p_{W|X, L, U}(w|x, l, u) dw.$$
 (2)

Assumption 8 (Treatment bridge): There exists  $g_0 \in \mathcal{L}^2(X, L, Z)$  such that for all  $(x, l, u) \in \text{supp}(X, L, U)$  satisfying that the map  $x' \mapsto q(x', l)$  is differentiable at x' = x,  $g_0$  is the solution to the integral equation

$$\alpha_0(x,l,u) = \int g(x,l,z) p_{Z|X,L,U}(z|x,l,u) dz, \qquad (3)$$

where

$$\alpha_0(x, l, u) = I\left\{x \in q\left([c(l), d(l)], l\right)\right\} \frac{dq^{-1}(x, l)}{dx} \frac{p_{X|L, U}\left\{q^{-1}(x, l) | l, u\right\}}{p_{X|L, U}(x|l, u)}.$$

The bridge functions can be viewed as counterparts to the outcome regression and density ratio functions in causal inference for MTPs under the assumption of no unmeasured confounders. The outcome bridge function coincides with the outcome bridge function needed for estimation of the average treatment effect (ATE) (Miao et al., 2018; Tchetgen Tchetgen et al., 2020). In contrast, the treatment bridge function is specific to our parameter of interest, namely the mean under an MTP.

When both the unmeasured confounder and the negative controls are discrete variables,

the existence of solutions to the integral equations (2) and (3) is guaranteed when certain matrices, defined by the conditional probabilities of the negative controls given the unmeasured confounder, have full column rank. For a comprehensive discussion of this topic, see Miao et al. (2018); Tchetgen Tchetgen et al. (2020); Shi et al. (2023); Cui et al. (2023), and Kallus et al. (2022).

In the continuous setting, these equations correspond to Fredholm integral equations of the first kind, which are known to be ill-posed. Such equations can be problematic, as they may lack solutions, have non-unique solutions, or possess solutions that do not depend continuously on the left-hand sides of the equations. In the Web appendix A, following Miao et al. (2018) and Cui et al. (2023), we invoke Piccard's Theorem (Theorem 15.18 in Kress (2010)) to argue that, under regularity conditions, the existence of an outcome bridge function  $h_0$  is ensured if the following completeness condition is satisfied for all  $(x, l) \in \text{supp}(X, L)$ :

$$\mathbb{E}\{\eta(X, L, U) | X = x, L = l, W\} = 0 \Rightarrow \eta(x, l, U) = 0 \quad \text{a.e.}$$
 (4)

Similarly, the existence of a treatment bridge function  $g_0$  is ensured, under regularity conditions, if the following completeness condition holds for all (x, l) in the support of (X, L) such that the map  $x' \mapsto q(x', l)$  is differentiable at x' = x:

$$\mathbb{E}\{\eta(X, L, U)|X = x, L = l, Z\} = 0 \Rightarrow \eta(x, l, U) = 0$$
 a.e. (5)

Completeness is a fundamental statistical concept, and in this context, indicates that the variability of the unmeasured confounder U is captured by the variability of the negative control variables. Specifically, for the completeness condition (4), the variability of U is captured by the variability of the negative control outcome W. For the completeness condition (5), the variability of U is captured by the variability of the negative control treatment Z. Following Kallus et al. (2022), we provide a result that links solutions to the latent

equations (2) and (3) with solutions of integral equations that depend solely on observed data.

THEOREM 1 (Observed Bridge Equations):

i) [Kallus, Mao, and Uehara (2022)] Under assumptions 4 and 5, any solution  $h_0(x, l, w)$  to equation (2) also solves, for all  $(x, l, z) \in \text{supp}(X, L, Z)$ , the following equation

$$\mathbb{E}(Y|X = x, L = l, Z = z) = \int h(x, l, w) p_{W|X, L, Z}(w|x, l, z) dw.$$
 (6)

ii) Under assumption 5, any solution to equation (3) also solves, for all  $(x, l, w) \in \text{supp}(X, L, W)$ , the following equation

$$\alpha_0(x, l, w) = \int g(x, l, z) p_{Z|X, L, W}(z|x, l, w) dz, \qquad (7)$$

where, with a slight abuse of notation,  $\alpha_0$  is defined as in equation (3) but with u replaced by w.

With these premises, building on the approaches of Miao et al. (2018); Cui et al. (2023); Tchetgen Tchetgen et al. (2020); Ghassami et al. (2022), and Kallus et al. (2022), we derive the following identification results for the MTP setting:

THEOREM 2 (Identification): Suppose assumptions 1 - 6 hold. If, in addition, either assumption 7 holds and equation (7) has at least one solution, or assumption 8 holds and equation (6) has at least one solution, then  $\psi_0$  satisfies all of the following:

*i)* (Outcome bridge representation)

$$\psi_{0} = \mathbb{E}\left[h^{\dagger}\left\{q\left(X,L\right),L,W\right\}\right],$$

where  $h^{\dagger}$  is any solution to equation (6).

ii) (Treatment bridge representation)

$$\psi_0 = \mathbb{E}\left\{Yg^{\dagger}\left(X, L, Z\right)\right\},\,$$

where  $g^{\dagger}$  is any solution to equation (7).

iii) (Double robust representation)

$$\psi_0 = \mathbb{E}\left\{\phi(O; h^{\dagger}, g^{\dagger})\right\},\,$$

where at least one of  $h^{\dagger}$  and  $g^{\dagger}$  solves the corresponding integral equations (6) and (7) respectively, and for any  $h \in \mathcal{L}^2(X, L, W)$  and  $g \in \mathcal{L}^2(X, L, Z)$ ,

$$\begin{split} \phi(O;h,g) := & \ h\left\{q\left(X,L\right),L,W\right\} \\ & + g(X,L,Z)\left\{Y-h(X,L,W)\right\}. \end{split}$$

Assertion i) of Theorem 2 was proved under slightly different assumptions than ours by Miao et al. (2018) and Kallus et al. (2022). Cui et al. (2023) and Kallus et al. (2022) obtained treatment bridge and double robust identifying representations for the ATE similar to those in assertions ii) and iii). In the Web Appendix A, we discuss the various assumptions proposed earlier and explain why ours is slightly different.

Note that when Z=W, the three representations of the counterfactual MTP mean in Theorem 2 align with the corresponding representations in the absence of unmeasured confounding (Diaz Munoz et al., 2012; Haneuse et al., 2013). Additionally, in line with standard double-robust identification results, the third representation in Theorem 2 is doublerobust because it requires only one of  $h^{\dagger}$  or  $g^{\dagger}$  to solve the corresponding observed equation to identify the target parameter, but not necessarily both.

Theorem 2 ensures that the target parameter remains identifiable even when multiple solutions exist for the observed integral equations (6) or (7). This key property was noted by Miao et al. (2018); Tchetgen Tchetgen et al. (2020) and Cui et al. (2023) under slightly different identifying assumptions and by Kallus et al. (2022) under identifying assumptions similar to ours for the generalized ATE.

### 4. Estimation

Our identification results suggest three potential estimators for the target parameter  $\psi_0$ . These estimators rely on the estimation of bridge functions, which serve as nuisance parameters. Let  $\mathbb{E}_n[\cdot]$  denote the empirical mean operator, i.e.,  $\mathbb{E}_n[t(O)] = \frac{1}{n} \sum_{i=1}^n t(O_i)$  for n i.i.d. copies  $O_1, \ldots, O_n$  of O, and let  $\|\cdot\|_{\infty}$  and  $\|\cdot\|_2$  denote the supreme norm and the norm in the corresponding  $\mathcal{L}^2(O)$  space, defined for any  $f \in \mathcal{L}^2(O)$  as  $\|f\|_{\infty} := \sup_{o \in \text{supp}(O)} |f(o)|$  and  $\|f\|_2 := [\mathbb{E}\{f(O)^2\}]^{1/2}$  respectively. Let  $\hat{h}$  and  $\hat{g}$  be estimators of the minimum  $\mathcal{L}^2$  norm solutions  $h_0$  and  $g_0$  of the bridge equations (6) and (7), respectively. Define the following three estimators of  $\psi_0$ :

$$\hat{\psi}^{OR} = \mathbb{E}_n \left[ \hat{h} \{ q(X, L), L, W \} \right],$$

$$\hat{\psi}^{IPW} = \mathbb{E}_n \left[ Y \hat{g}(X, L, Z) \right], \quad \text{and}$$

$$\hat{\psi}^{DR} = \mathbb{E}_n \left[ \phi(O; \hat{h}, \hat{g}) \right].$$

The estimators  $\hat{\psi}^{OR}$  and  $\hat{\psi}^{IPW}$  do not generally achieve  $\sqrt{n}$ -consistency unless  $\hat{h}$  and  $\hat{g}$  converge to  $h_0$  and  $g_0$  at parametric rates. However, parametric rates can only be obtained under correctly specified parametric models for the unknown bridge functions, and such models are seldom correct in practice. Due to this limitation, we focus exclusively on the doubly-robust estimator, for which we provide an asymptotic analysis without assuming that the bridge functions are confined to parametric models.

## 4.1 Estimation Procedure

Following the modern theory of debiased machine learning (Chernozhukov et al., 2018), we analyze a cross-fitted version of the estimator  $\hat{\psi}^{DR}$ . For both  $\hat{\psi}^{DR}$  and its cross-fitted version to converge to a normal distribution with mean zero at a  $\sqrt{n}$  rate, a certain remainder term—defined later—must be of order  $o_p(n^{-1/2})$ . The estimator  $\hat{\psi}^{DR}$  further requires that the functions  $h_0$  and  $g_0$ , along with their estimators, lie within function classes subject to

specific size constraints, such as Donsker classes. In contrast, this condition is not necessary for the cross-fitted version of  $\hat{\psi}^{DR}$  to achieve  $\sqrt{n}$  convergence. We focus on the cross-fitted estimator because this relaxation broadens the set of data-generating processes under which the estimator of the target parameter is asymptotically normal.

Let  $I_1, \ldots, I_K$  represent a partition of the sample into K equal-sized parts. For each  $k \in \{1, \ldots, K\}$ , using data from all parts except  $I_k$ , we obtain estimators  $\hat{h}^{(-k)}$  and  $\hat{g}^{(-k)}$  for the bridge functions  $h_0$  and  $g_0$ . We define  $\hat{\psi}_k$  as:

$$\hat{\psi}_k = \frac{1}{|I_k|} \sum_{i:O_i \in I_k} \phi \left\{ O_i; \hat{h}^{(-k)}, \hat{g}^{(-k)} \right\}.$$

Our final estimator of  $\psi_0$  is given by:

$$\hat{\psi}_{CF}^{DR} = \frac{1}{K} \sum_{k=1}^{K} \hat{\psi}_k.$$
 (8)

We now present the asymptotic properties of our doubly-robust cross-fitted estimator.

THEOREM 3: Let  $h_0$  and  $g_0$  denote the minimum-norm solutions of the integral equations (6) and (7), respectively. If  $|\alpha_0(X, L, W)| \leq B$ ,  $|Y| \leq B$ , either  $||h_0||_{\infty} + ||\hat{g}||_{\infty} \leq B$  or  $||\hat{h}||_{\infty} + ||g_0||_{\infty} \leq B$  for some B, and the estimators  $\hat{h}^{(-k)}$  and  $\hat{g}^{(-k)}$  are norm consistent in the sense that  $||\hat{h}^{(-k)} - h_0||_2 = o_p(1)$  and  $||\hat{g}^{(-k)} - g_0||_2 = o_p(1)$  for all  $k \in \{1, \ldots, K\}$ , then the estimator  $\hat{\psi}_{CF}^{DR}$  satisfies

$$\sqrt{n} \left( \hat{\psi}_{CF}^{DR} - \psi_0 \right) = \sqrt{n} \mathbb{E}_n \left[ \phi(O; h_0, g_0) - \psi_0 \right] + \sqrt{n} R_n + o_p(1),$$

where

$$R_n = \frac{1}{K} \sum_{k=1}^{K} \mathbb{E} \left[ \left\{ \hat{h}^{(-k)} - h_0 \right\} \left\{ g_0 - \hat{g}^{(-k)} \right\} \right].$$

In particular, if  $R_n = o_p(n^{-1/2})$  and  $\mathbb{E}\left\{\phi(O; h_0, g_0)^2\right\} < \infty$ , then

$$\sqrt{n} \left( \psi_{CF}^{DR} - \psi_0 \right) \stackrel{d}{\longrightarrow} \mathcal{N}(0, \tau^2),$$
(9)

where  $\tau^2 = \mathbb{E}\left[ \{ \phi(O; h_0, g_0) - \psi_0 \}^2 \right]$ .

In the next section, we construct non-parametric estimators  $\hat{h}^{(-k)}$  and  $\hat{g}^{(-k)}$  that under

certain assumptions, are norm consistent and yield  $R_n = o_p (n^{-1/2})$  and consequently result in  $\hat{\psi}_{CF}^{DR}$  asymptotically linear. The expression for  $\tau^2$  suggests estimating it with

$$\hat{\tau}^2 = \frac{1}{n} \sum_{k=1}^K \sum_{i:O_i \in I_k} \left[ \phi \left\{ O_i; \hat{h}^{(-k)}, \hat{g}^{(-k)} \right\} - \hat{\psi}_{CF}^{DR} \right]^2$$

Under regularity conditions,  $\hat{\tau}^2$  is a consistent estimator of  $\tau^2$  that can be used to construct Wald confidence intervals centered at  $\hat{\psi}_{CF}^{DR}$ .

## 4.2 Estimation of the Bridge Functions

To estimate the observed bridge functions, we adopt a recent method (Dikkala et al., 2020; Chernozhukov et al., 2020; Ghassami et al., 2022; Bennett et al., 2023), which reformulates the observed bridge equations as minimax problems over specific function classes. This method has gained attention because it bypasses the need to estimate the conditional mean operators, a difficult task when conditioning on vectors with continuous covariates, due to the curse of dimensionality. As noted in Bennett, Kallus, and Schnabel (2019); Muandet et al. (2020); and Ghassami et al. (2022), the key insight for the approach lies in the following result that is shown in Web Appendix E for completeness.

LEMMA 1: Suppose that V is a random vector and  $V_d$  and  $V_f$  are two distinct subvectors of V, not necessarily disjoint. Let  $m: \mathcal{L}^2(V_f) \times \text{supp}(V) \to \mathcal{L}^2(V)$  be a known mapping such that the functional  $f \in \mathcal{L}^2(V_f) \mapsto \mathbb{E} \{m(f; V)\}$  is bounded and linear with Riesz representer  $\beta(V_f)$ . Suppose that  $d_0 \in \mathcal{L}^2(V_d)$  satisfies

$$r_2(V_f)\mathbb{E}\left\{d_0(V_d)r_1(V)|V_f\right\} = \beta(V_f)$$
 (10)

for given fixed  $r_1 \in \mathcal{L}^2(V)$  and  $r_2 \in \mathcal{L}^2(V_f)$  such that  $r_2(v_f)^2 = r_2(v_f)$  for all  $v_f \in \text{supp}(V_f)$ . Then, for any c > 0 and any  $d \in \mathcal{L}^2(V_d)$ , it holds that

$$\max_{f \in \mathcal{L}^{2}(V_{f})} \mathbb{E} \left\{ m(f; V) - d(V_{d}) r_{1}(V) r_{2}(V_{f}) f(V_{f}) - c \cdot r_{2}(V_{f}) f(V_{f})^{2} \right\}$$

$$= \frac{1}{4c} \mathbb{E} \left\{ r_{2}(V_{f}) \mathbb{E} \left[ \left\{ d_{0}(V_{d}) - d(V_{d}) \right\} r_{1}(V) | V_{f} \right]^{2} \right\}.$$

Consequently,  $d_0$  belongs to

$$\arg \min_{d \in \mathcal{L}^{2}(V_{d})} \max_{f \in \mathcal{L}^{2}(V_{f})} \mathbb{E}\left\{m(f; V) - d(V_{d}) r_{1}(V) r_{2}(V_{f}) f(V_{f}) - c \cdot r_{2}(V_{f}) f(V_{f})^{2}\right\}. \tag{11}$$

Furthermore, any other  $d_1$  in (11) also satisfies equation (10).

In our setting, V = (X, L, Z, W, Y). Taking  $V_d = (X, L, W)$ ,  $V_f = (X, L, Z)$ ,  $r_1(V) = 1$ ,  $r_2(V_f) = 1$ ,  $m(f; V) = Yf(V_f)$ , and  $\beta(V_f) = \mathbb{E}(Y|X, L, Z)$ , equation (10) corresponds to the outcome bridge equation (6). Similarly, taking  $V_d = (X, L, Z)$ ,  $V_f = (X, L, W)$ ,  $r_1(V) = 1$ ,  $r_2(V_f) = I\{X \in q([c(L), d(L)], L)\}$ ,  $m(f; V) = f\{q(X, L), L, W\}$ , and  $\beta(V_f) = \alpha_0(X, L, W)$ , equation (10) becomes equivalent to the treatment bridge equation (7). Remarkably, the preceding Lemma shows that it is possible to characterize the solutions of the equations (6) and (7) as solutions to the minimax problem (11) which does not involve the computation of the conditional mean expectation of functions of V given  $V_f$ .

Inspired by Lemma 1 and building on the works of Dikkala et al. (2020) and Ghassami et al. (2022), we propose estimating  $h_0$  and  $g_0$  as follows. Let  $\mathcal{H}, \mathcal{H}' \subseteq \mathcal{L}^2(X, L, W)$  and  $\mathcal{G}, \mathcal{G}' \subseteq \mathcal{L}^2(X, L, Z)$  denote function classes, each of them included in, possibly distinct, reproducing kernel Hilbert spaces specified by the data analyst. For each  $k \in \{1, \ldots, K\}$ , the estimators of the bridge functions are defined as:

$$\hat{h}^{(-k)} = \arg\min_{h \in \mathcal{H}} \max_{g \in \mathcal{G}'} \left\{ \Psi_{H,n}^{(-k)}(h,g) - \lambda_{\mathcal{G}'} \|g\|_{\mathcal{G}'}^2 + \lambda_{\mathcal{H}} \|h\|_{\mathcal{H}}^2 \right\}, \tag{12}$$

$$\hat{g}^{(-k)} = I_q(X, L) \cdot \arg\min_{g \in \mathcal{G}} \max_{h \in \mathcal{H}'} \left\{ \Psi_{G,n}^{(-k)}(g, h) - \lambda_{\mathcal{H}'} ||h||_{\mathcal{H}'}^2 + \lambda_{\mathcal{G}} ||g||_{\mathcal{G}}^2 \right\}, \tag{13}$$

where  $I_q(X,L) := I\{X \in q([c(L),d(L)],L)\}, \lambda_{\mathcal{H}}, \lambda_{\mathcal{H}'}, \lambda_{\mathcal{G}}, \text{ and } \lambda_{\mathcal{G}'} \text{ are positive tuning parameters,}$ 

$$\begin{split} &\Psi_{H,n}^{(-k)}(h,g) = \mathbb{E}_n^{(-k)} \big[ g(X,L,Z) \left\{ Y - h(X,L,W) \right\} - g(X,L,Z)^2 \big], \\ &\Psi_{G,n}^{(-k)}(g,h) = \mathbb{E}_n^{(-k)} \big[ h \left\{ q(X,L),L,W \right\} - I_q(X,L)h(X,L,W)g(X,L,Z) - I_q(X,L)h(X,L,W)^2 \big], \\ &\text{and } \mathbb{E}_n^{(-k)} \text{ denotes the empirical expectation over data excluding the } I_k \text{ fold. The norms} \\ &\| \cdot \|_{\mathcal{H}}, \| \cdot \|_{\mathcal{H}'}, \| \cdot \|_{\mathcal{G}}, \text{ and } \| \cdot \|_{\mathcal{G}'} \text{ are the norms of the reproducing kernel Hilbert spaces where} \end{split}$$

 $\mathcal{H}$ ,  $\mathcal{H}'$ ,  $\mathcal{G}$ , and  $\mathcal{G}'$  are included. Although the estimators  $\hat{h}^{(-k)}$  and  $\hat{g}^{(-k)}$  can be defined for arbitrary normed function classes  $\mathcal{H}$ ,  $\mathcal{H}'$ ,  $\mathcal{G}$  and  $\mathcal{G}'$ , in this paper we focus on function classes of reproducing kernel Hilbert spaces because the estimators admit closed form expressions. We provide these expressions in Section 4.3.

Our estimator of  $h_0$  aligns with those of Dikkala et al. (2020) and Ghassami et al. (2022), but our estimator for  $g_0$  is specific to the MTP setting. Although we use a similar penalization strategy, our convergence analysis relies on different assumptions. Unlike Dikkala et al. (2020) and Ghassami et al. (2022), who require uniqueness of the solutions to the observed equations (6) and (7) to obtain remainder terms of order  $o_p(n^{1/2})$ , our analysis adapts the framework of Bennett et al. (2023). Specifically, we show that our estimators converge to the minimumnorm solutions of the observed equations (6) and (7), even when these equations admit multiple solutions. To enhance computational stability and avoid inverting near-singular matrices of large dimension, we penalize the inner maximization terms using  $\lambda_{\mathcal{G}'} ||g||_{\mathcal{G}'}^2$  and  $\lambda_{\mathcal{H}'} ||h||_{\mathcal{H}'}^2$  (see Section 4.3 for an explanation of this). This strategy contrasts with the approach of Bennett et al. (2023), who penalize only the outer minimizations.

In the Web appendix B, we provide bounds on the rates of convergence of  $\hat{h}^{(-k)}$  and  $\hat{g}^{(-k)}$  to  $h_0$  and  $g_0$  under regularity conditions that include the requirement that the minimum-norm solutions  $h_0$  and  $g_0$  are smooth in the sense of satisfying the  $\beta$ -source condition with  $\beta \geq 1$ . While the  $\beta$ -source condition is standard for deriving rates of convergence of estimators of minimum norm solutions to integral equations like the outcome and treatment bridge equations (6) and (7) (Carrasco et al., 2007), our formulation is tailored to estimators based on reproducing kernel Hilbert spaces. We show that, under regularity conditions and for  $\mathcal{H}$ ,  $\mathcal{H}'$ ,  $\mathcal{G}$  and  $\mathcal{G}'$  in reproducing kernel Hilbert spaces with Gaussian kernels, selecting  $\lambda_{\mathcal{H}}$  and  $\lambda_{\mathcal{G}}$  to converge to 0 at the rate  $O\left(\log(n)/n\right)$ , and  $\lambda_{\mathcal{H}'}$  and  $\lambda_{\mathcal{G}'}$  to converge to 0 at the rate  $O\left(\log(n)/n\right)$ , results in estimators of the bridge functions such that the remainder term  $R_n$ 

is  $o_p(n^{-1/2})$ . Consequently, with these choices the estimator  $\psi_{CF}^{DR}$  is asymptotically normal with limiting distribution given in Theorem 3. Strategies for selecting the tuning parameters in practice to achieve the desired optimal values remain an open problem, the investigation of which is beyond the scope of this paper. While a natural approach is to select the tuning parameters by cross-validation, a key challenge lies in the choice of the risk estimator to minimize. See Section 5 for the strategy we used in the simulations and data analysis to select the tuning parameters.

# 4.3 Closed-Form Expressions for the Estimators $\hat{h}^{(-k)}$ and $\hat{g}^{(-k)}$

To simplify notation, in this section we omit the superscript (-k) from the estimators of the bridge functions and denote with n the size of the sample from which they are computed. Let  $K_{\mathcal{H}}$ ,  $K_{\mathcal{H}'}$ ,  $K_{\mathcal{G}}$ , and  $K_{\mathcal{G}'}$  denote the kernel functions associated with the reproducing kernel Hilbert spaces and let  $K_{\mathcal{H},n}$ ,  $K_{\mathcal{H}',n}$ ,  $K_{\mathcal{G},n}$ , and  $K_{\mathcal{G}',n}$  be the  $n \times n$  matrices whose (i,j)-th entry corresponds to the value of the respective kernel function evaluated at observations i and j. By the representer Theorem (Schölkopf, Herbrich, and Smola, 2001),  $\hat{h}$  and  $\hat{g}$  admit closed form expressions which are given by:

$$\hat{h}(x, l, w) = \sum_{j=1}^{n} \gamma_{j} K_{\mathcal{H}} \left\{ (x, l, w), (x_{j}, l_{j}, w_{j}) \right\},$$

$$\hat{g}(x, l, z) = I \left\{ x \in [c(l), d(l)] \right\} \cdot \sum_{j=1}^{n} \theta_{j} K_{\mathcal{G}} \left\{ (x, l, z), (x_{j}, l_{j}, z_{j}) \right\},$$

for some constants  $\gamma_j$  and  $\theta_j$ ,  $j=1,\ldots,n$ . In the Web Appendix B we show that  $\gamma:=(\gamma_1,\ldots,\gamma_n)$  and  $\theta:=(\theta_1,\ldots,\theta_n)$  are given by:

$$\gamma = \left(K_{\mathcal{H},n} \Gamma_{\mathcal{G}'} K_{\mathcal{G}',n} K_{\mathcal{H},n} + n^2 \lambda_{\mathcal{H}} K_{\mathcal{H},n}\right)^{\dagger} K_{\mathcal{H},n} \Gamma_{\mathcal{G}'} K_{\mathcal{G}',n} \tilde{Y}_n,$$

$$\theta = \left(K_{\mathcal{G},n} R_n \Gamma_{\mathcal{H}'} K_{\mathcal{H}',n} R_n K_{\mathcal{G},n} + n^2 \lambda_{\mathcal{G}} K_{\mathcal{G},n}\right)^{\dagger} K_{\mathcal{G},n} R_n \Gamma_{\mathcal{H}'} \tilde{K}_{\mathcal{H},n}^T \mathbf{1}_n,$$

and † denotes the Moore-Penrose pseudoinverse. Here,  $\tilde{Y}_n = (y_1, \dots, y_n)^T$  is the vector of observed outcomes,  $1_n = (1, \dots, 1)^T$  is the vector of ones,  $R_n$  is the  $n \times n$  diagonal matrix with values  $I\{x_i \in q(\mathcal{S}(l_i), l_i)\}$  for  $i = 1, \dots, n$ , in its diagonal, and  $\tilde{K}_{\mathcal{H},n}$  is the  $n \times n$  matrix

with (i, j)-entry given by  $K_{\mathcal{H}'}\{(q(x_i, l_i), l_i, w_i), (x_j, l_j, w_j)\}$ . The matrices  $\Gamma_{\mathcal{G}'}$  and  $\Gamma_{\mathcal{H}'}$  are defined as:

$$\Gamma_{\mathcal{G}'} = \frac{1}{4} \left[ \frac{1}{n} K_{\mathcal{G}',n} + \lambda_{\mathcal{G}'} I_n \right]^{-1}$$

and

$$\Gamma_{\mathcal{H}'} = \frac{1}{4} \left[ \frac{1}{n} K_{\mathcal{H}',n} R_n + \lambda_{\mathcal{H}'} I_n \right]^{-1}$$

where  $I_n$  is the  $n \times n$  identity matrix. Notice that if  $\lambda_{\mathcal{G}'}$  and  $\lambda_{\mathcal{H}'}$  were set to zero, the computation of  $\Gamma_{\mathcal{G}'}$  and  $\Gamma_{\mathcal{H}'}$  would involve inverting the near singular  $n \times n$  matrices  $K_{\mathcal{G}',n}$  and  $K_{\mathcal{H}',n}$  thus resulting in unstable estimators. In contrast, addition of  $\lambda_{\mathcal{G}'}I_n$  and  $\lambda_{\mathcal{H}'}I_n$  for  $\lambda_{\mathcal{G}'}$  and  $\lambda_{\mathcal{H}'}$  of magnitude roughly 1/n results in matrices  $\frac{1}{n}K_{\mathcal{G}',n} + \lambda_{\mathcal{G}'}I_n$  and  $\frac{1}{n}K_{\mathcal{H}',n}R_n + \lambda_{\mathcal{H}'}I_n$  with eigenvalues bounded away from zero. This supports our earlier assertion that regularizing the inner maximization with the squared of the class norm of the function stabilizes the computations.

### 5. Numerical experiments

We evaluated the finite-sample performance of our doubly-robust cross-fitted kernel estimator via simulations based on data generated with varying levels of correlation between the negative controls, Z and W, and the unmeasured confounder U, conditioned on observed confounders L. To illustrate the advantages of our estimator, we compare its performance to two existing doubly-robust estimators for the counterfactual MTP mean in the absence of unmeasured confounding (Diaz Munoz et al., 2012; Diaz et al., 2023): the augmented inverse probability weighted estimator (Non-proximal AIPW) and the targeted minimum loss-based estimator (Non-proximal TMLE).

Let  $\mathcal{TN}_{[a,b]}(\mu, \sigma^2)$  denote the probability distribution obtained from truncating a normally distributed variable  $\mathcal{N}(\mu, \sigma^2)$  within the interval [a, b], and let  $\mathcal{TN}_c(\mu, \sigma^2)$  denote a specific case where  $a = \mu - 3\sigma$  and  $b = \mu + 3\sigma$ . For each i = 1, ..., n, we generated variables

with bounded support as follows: the observed confounder  $L_i \sim T \mathcal{N}_c(0,1)$ , the unobserved confounder  $U_i \sim \mathcal{TN}_c(0.5L_i, 1)$ , the negative controls  $Z_i \sim \mathcal{TN}_c(0.2L_i + \beta_z U_i, 1)$  and  $W_i \sim \mathcal{TN}_c(0.5L_i + \beta_w U_i, 1)$ , the exposure  $X_i \sim \mathcal{TN}_{[-2,2]}(0.3L_i + U_i, 1)$ , and the outcome  $Y_i \sim \text{Bernoulli}(p_i) \text{ where } p_i = \{1 + \exp(1 - 0.5L_i + U_i + 1.5X_i + 0.75X_i^2)\}^{-1}. \text{ Here, the}$ parameters  $\beta_z$  and  $\beta_w$  control the conditional correlation of the negative controls with the unmeasured confounder U. Specifically, we generated data across nine scenarios by combining  $\beta_z \in \{2, 1, 0.5\}$  and  $\beta_w \in \{-2, -1, -0.5\}$ . These values correspond to conditional correlations of Cor(Z, U|L) = 0.894, 0.707, and 0.447 for  $\beta_z$ , and Cor(W, U|L) = -0.894, -0.707, and -0.447 for  $\beta_w$ . These scenarios allow us to examine how different levels of conditional correlation between negative controls and the unmeasured confounder affect the estimator's performance. The estimation target is  $\mathbb{E}\left[Y\left\{q(X)\right\}\right]$  for  $q(x)=x+0.4\cdot I\left\{-2\leqslant x\leqslant 0.6\right\}+1$  $\frac{0.4(2-x)}{1.4} \cdot I$  {0.6 <  $x \le 2$ }, which under all the data generating scenarios is equal to 0.2512. Here q(x) is the shift intervention policy described in Example 2, with a shift  $\delta = 0.4$  and  $\varepsilon = 1$ . The data-generating mechanism and policy satisfy assumptions 1-8, as well as the conditions required by Theorem 3. Notably, the exposure X has a fixed support, ensuring that its support does not change with U. The outcome and treatment bridge functions are provided in Web Appendix C.

We examined the performance of the doubly-robust cross-fitted estimator  $\hat{\psi}_{CF}^{DR}$  with bridge functions estimated as in (12) and (13) where the function classes  $\mathcal{H}$ ,  $\mathcal{G}'$ ,  $\mathcal{G}$ , and  $\mathcal{H}'$  were Gaussian reproducing kernel Hilbert spaces. Since Gaussian kernels rely on distances between observations, differences in the scale of the observed confounder L,or the negative controls Z and W, could lead to an imbalance in their contributions to the kernel's distance computation. To prevent any of these variables from disproportionately influencing the estimation due to differences in scale, we standardized them before implementing the estimation procedure. We used 3-fold cross-fitting. Specifically, we randomly split the sample into three equally

sized folds, designating fold 1 to the first fold, fold 2 to the second and fold 3 to the third. For subjects in fold 1, we estimated the bridge functions as follows. In fold 2, we estimated the bridge functions for fixed specified hyperparameters  $(\lambda_{\mathcal{H}}, \lambda_{\mathcal{G}'}, \lambda_{\mathcal{G}}, \lambda_{\mathcal{H}'})$  with  $\lambda_{\mathcal{H}} \, = \, c_1 \left\{ \frac{\log(n)}{n} \right\}^{1/2}, \; \lambda_{\mathcal{G}'} \, = \, c_2 \frac{\log(n)}{n}, \; \lambda_{\mathcal{G}} \, = \, c_3 \left\{ \frac{\log(n)}{n} \right\}^{1/2}, \; \text{and} \; \; \lambda_{\mathcal{H}'} \, = \, c_4 \frac{\log(n)}{n}, \; \text{where} \; \, c_1, c_3 \, \in \, c_4 \frac{\log(n)}{n}, \; c_5 \frac{\log(n)}{n}, \; c_6 \frac{\log(n)}$  $\{10^{-5}, 10^{-4}, 10^{-3}, 10^{-2}, 10^{-1}\}\$ and  $c_2, c_4 \in \{0.1, 1, 10, 100\},\$ and fixed specified bandwidths  $(\sigma_{\mathcal{H}}^2, \sigma_{\mathcal{G}'}^2, \sigma_{\mathcal{G}}^2, \sigma_{\mathcal{H}'}^2)$ . The bandwidth  $\sigma_{\mathcal{G}'}^2$  was fixed at 1/4 times the median of the pairwise euclidean distance between the observed vectors  $(X_i, L_i, Z_i)$  (Garreau, Jitkrittum, and Kanagawa, 2017). Likewise,  $\sigma_{\mathcal{H}'}^2$  was fixed at 1/4 times the median of the pairwise euclidean distance between the observed vectors  $(X_i, L_i, W_i)$ . The bandwidths  $\sigma_{\mathcal{H}}^2$  and  $\sigma_{\mathcal{G}}^2$  were also computed with the median of the pairwise Euclidean distances between observations, but multiplied by  $c_5 \in \{1/4, 1/2, 1, 2, 4\}$ . In fold 3, we selected the hyperparameter configuration  $(\lambda_{\mathcal{H}}, \lambda_{\mathcal{G}'}, \lambda_{\mathcal{G}}, \lambda_{\mathcal{H}'})$  and the bandwidth pair  $(\sigma_{\mathcal{H}}^2, \sigma_{\mathcal{G}}^2)$  that minimized a specific empirical loss function detailed in Web Appendix C. The bridge functions for units in fold 1 were those estimated in fold 2 with the hyperparameter configuration and bandwidth pair selected in fold 3. For subjects in fold 2 (fold 3), the bridge functions were estimated analogously using fold 1 (fold 2) to select the hyperparameter configuration and bandwidth pair, and fold 3 (fold 1) to estimate the bridge functions. The final estimator of the MTP mean was computed as in (8).

For implementing the non-proximal MTP estimators of Diaz Munoz et al. (2012) and Diaz et al. (2023), we used the open-source R package 1mtp with several libraries for estimation of the outcome regression and density ratio functions. In addition to adjusting for the observed confounder L, the non-proximal estimators also adjusted for the negative controls Z and W, which correspond to precision variables under the specified data-generating mechanisms. We considered these adjustments important to ensure a fair comparison with the proximal estimators.

The preceding process was repeated 500 times for sample sizes  $n \in \{750, 1500, 3000, 6000\}$ . The performance of our estimator (Proximal DR) and its competitors is summarized in Figure 2. In most of the scenarios considered, the estimator  $\hat{\psi}_{CF}^{DR}$  exhibits low bias, with the average estimated asymptotic variance closely aligning with the empirical variance of  $\hat{\psi}_{CF}^{DR}$ . The coverage of the confidence intervals remains very close to the nominal level. Our estimator outperforms the non-proximal estimators in terms of bias and coverage, with the performance gap narrowing as the conditional correlation between the negative controls and the unmeasured confounder decreases. Additionally, across the sample sizes studied, the performance of the  $\hat{\psi}_{CF}^{DR}$  declines as the degree of conditional correlation between the negative controls and the unmeasured confounder weakens. This is expected, as weaker correlations imply that the negative controls provide less information about the unmeasured confounder, making the estimation of the bridge functions more challenging and requiring larger sample sizes for the finite sample distribution of  $\hat{\psi}_{CF}^{DR}$  be well approximated by its asymptotic distribution.

In Web Appendix C, we also present results for a doubly-robust estimator that employs parametric estimators of the bridge functions. These simulations illustrate that estimation of the counterfactual MTP mean also deteriorates as the conditional correlation between the negative controls and the unmeasured confounder weakens, even when the estimation is based on correctly specified parametric models for the bridge functions.

[Figure 2 about here.]

### 6. Application

We applied our methodology to investigate neutralizing antibody levels 29 days (D29) post-vaccination as correlates of protection against symptomatic COVID-19 infection in the ENSEMBLE trial. Our analysis is based on vaccine recipients that met the per-protocol

criteria and were SARS-CoV-2 seronegative at baseline. Specifically, it was based on 1,164 vaccine recipients who had neutralizing antibody measurements at D29. These participants were selected using a two-phase case-cohort sampling design, as outlined in the statistical analysis plan by Gilbert et al. (2022b). To account for this sampling design, we employed a weighted version of our estimator, as detailed in Web Appendix B. To avoid potential violations of the positivity assumption, we limited our analysis to countries where at least 50 participants had D29 antibody measurements, thus limiting our analysis to six of the eight countries where the trial was conducted. The outcome of interest was a binary indicator of developing symptomatic, molecularly confirmed COVID-19 infection with onset between 7 and 210 days after D29. During this follow-up period, 366 symptomatic COVID-19 cases were observed among vaccine recipients with antibody measurements.

In our analysis we included the baseline covariates (L) age, geographic region, and a prespecified risk score for acquiring symptomatic COVID-19. Anti-Spike binding antibody levels served as a negative control treatment, while the burden of respiratory symptoms unrelated to SARS-CoV-2 infection during follow-up was employed as a negative control outcome. We computed the burden of respiratory symptoms as the average number of symptoms per day that were not attributed to SARS-CoV-2, calculated during periods when participants reported symptoms and normalized by the maximum of these averages within each country. This normalization accounted for seasonal variations in respiratory symptoms during the trial follow-up across the different countries involved.

We assessed the effect of five shift intervention policies, as described in Example 2, with  $\delta \in \{0.2, 0.4, 0.6, 0.8, 1\}$ ,  $\varepsilon \equiv 1$ , and assuming that  $c(\cdot)$  and  $d(\cdot)$  are constant functions. Among the vaccine recipients analyzed, neutralizing antibody levels at D29 (log10 scale) ranged from 0.3889 to 4.2175. For the five policy interventions, the percentages of vaccine recipients whose observed antibody levels fell in the image of each policy were 42.5%, 38.2%, 27.3%,

18.8%, and 11.3%, respectively. We implemented our doubly-robust cross-fitted estimator using the same number of folds, function classes, and tuning parameters for estimating the bridge functions as those employed in our numerical experiments described in Section 5.

The observed probability of symptomatic COVID-19 infection between 7 and 210 days after D29 for the analyzed sample was 0.0235, (95% CI 0.0204 - 0.0265). Under a policy that increases each participant's antibody levels by one logarithmic unit, the probability of COVID-19 infection during this time decreased to 0.0094 (95% CI 0.0042 - 0.0145). Figure 3 presents the results for the policies that shift antibody levels by 0.2, 0.4, 0.6, 0.8, and 1 logarithmic unit from their observed values as described in Example 2.

Additionally, we computed the counterfactual vaccine efficacy under each of the five policies. Vaccine efficacy (VE) is a widely used measure that quantifies the relative reduction in disease cumulative incidence between a hypothetical world where everyone receives the vaccine and one where everyone receives the placebo. It is defined as  $VE := 1 - \mathbb{E}\{Y(A=1)\}/\mathbb{E}\{Y(A=0)\}$ , where A indicates whether an individual is a vaccine recipient. In our case, a relevant related quantity is

$$VE(q) = 1 - \frac{\mathbb{E}[Y\{A = 1, q(X)\}]}{\mathbb{E}\{Y(A = 0)\}}.$$

This quantifies the relative reduction in the probability of symptomatic COVID-19 infection between a hypothetical world where everyone receives the vaccine and develops neutralizing antibody levels according to the specified policy q and one where everyone receives placebo. To compute this estimand, we used data from 17,108 placebo recipients from the same six countries as the analyzed vaccine recipients, assigning them a neutralizing antibody level of zero based on prior structural knowledge. Among these placebo recipients, there were 805 COVID-19 cases during the same follow-up period, resulting in an observed probability of symptomatic COVID-19 infection of 0.0471 (95% CI 0.0439 - 0.0503). Combining this information with that from the analyzed vaccine recipients, the observed VE in the trial was

0.502 (95% CI 0.428 - 0.575). Under a policy that increases each participant's antibody levels by one logarithmic unit, the VE improved to 0.801 (95% CI 0.745 - 0.857). Vaccine efficacy estimates for the other policies are also presented in Figure 3.

## [Figure 3 about here.]

### 7. Discussion

In this study, we provided proximal identification conditions for causal estimands involving modified treatment policies and developed an asymptotically normal cross-fitted estimator based on non-parametric estimators of the observed bridge functions. We estimated the bridge functions using the recently proposed reformulation of the observed bridge equations as minimax optimization problems. Specifically, we solve regularized versions of these minimax problems over reproducing kernel Hilbert spaces and introduced a novel beta source condition tailored for these spaces, which under certain conditions provides desired convergence guarantees for the estimators without requiring unique solutions. Furthermore, we implemented our estimator on policies that are interpretable and satisfy positivity conditions.

We illustrated our methodology through numerical experiments and a real data application. In numerical experiments, our estimator outperformed conventional non-proximal methods across a range of scenarios with different levels of correlation between the negative controls and the unmeasured confounder. This advantage becomes particularly relevant in immuno-bridging trials, where an individual's immunity level serves as an unobserved confounder. Compared to existing non-proximal estimators, our approach provides a more reliable method for identifying true correlates of protection.

A future research direction is to extend this work to handle censored outcomes, which are common in observational studies and central to survival analysis. Censored data provide valuable insights into the time to event, even when the exact event time is unobserved,

preventing bias from excluding participants who have not yet experienced the event. Another research direction is to accommodate longitudinal modified treatment policies which would enable the optimization of sequential treatment decisions while accounting for time-varying confounding.

#### ACKNOWLEDGEMENTS

The authors thank.

### References

- Bennett, A., Kallus, N., and Schnabel, T. (2019). Deep generalized method of moments for instrumental variable analysis. *Advances in Neural Information Processing Systems* **32**, 3564–3574.
- Bennett, A., Kallus, N., Mao, X., Newey, W., Syrgkanis, V. and Uehara, M. (2023). Source condition double robust inference on functionals of inverse problems. Preprint 2023, arXiv:2307.13793.
- Carrasco, M., Florens, J.P., Renault, E. (2007). Linear inverse problems in structural econometrics estimation based on spectral decomposition and regularization. *Handbook of econometrics* **6**, 5633–5751.
- Chernozhukov, V., Chetverikov, D., Demirer, M., Duflo, E., Hansen, C., Newey, W., et al. (2018). Double/debiased machine learning for treatment and structural parameters.

  Econometrics Journal 21, C1–C68.
- Chernozhukov, V., Newey, W., Singh, R., and Syrgkanis, V. (2020). Adversarial Estimation of Riesz Representers. Preprint, arXiv:2101.00009v1.
- Cui, Y., Pu, H., Shi, X., Miao, W., and Tchetgen Tchetgen, E. J. (2023). Semiparametric proximal causal inference. *Journal of the American Statistical Association*, 1-12.

- Diaz Munoz, I. and van der Laan, M. (2012). Population intervention causal effects based on stochastic interventions. *Biometrics* **68**, 541–549.
- Díaz, I., Williams, N., Hoffman, K. L., and Schenck, E. J. (2023). Nonparametric causal effects based on longitudinal modified treatment policies. *Journal of the American Statistical Association* **118**, 846–857.
- Dikkala, N., Lewis, G., Mackey, L., and Syrgkanis, V. (2020). Minimax estimation of conditional moment models. Advances in Neural Information Processing Systems 33, 12248-12262.
- Feng, S., Phillips, D.J., White, T., Sayal, H., Aley, P.K., Bibi, S., et al. (2021). Correlates of protection against symptomatic and asymptomatic SARS-CoV-2 infection. *Nature medicine* 27, 2032–2040.
- Fleming, T.R., and Powers, J.H. (2012). Biomarkers and surrogate endpoints in clinical trials. Statistics in medicine 31, 2973–2984.
- Fong, Y., McDermott, A. B., Benkeser, D., Roels, S., Stieh, D. J., Vandebosch, A., et al. (2022). Immune correlates analysis of the ENSEMBLE single Ad26. COV2. S dose vaccine efficacy clinical trial. *Nature microbiology* 7, 1996–2010.
- Fong, Y., Huang, Y., Benkeser, D., Carpp, L.N., Áñez, G., Woo, W., et al. (2023). Immune correlates analysis of the PREVENT-19 COVID-19 vaccine efficacy clinical trial. *Nature communications* 14, 331.
- Garreau, D., Jitkrittum, W., and Kanagawa, M. (2017). Large sample analysis of the median heuristic. Preprint, arXiv:1707.07269.
- Ghassami, A. E., Ying, A., Shpitser, I., and Tchetgen Tchetgen, E.J. (2022). Minimax kernel machine learning for a class of doubly robust functionals with application to proximal causal inference. Preprint 2022, arXiv:2104.02929v3.
- Gilbert, P. B., Donis, R. O., Koup, R. A., Fong, Y., Plotkin, S. A., Follmann, D. A Covid-

- 19 Milestone Attained A Correlate of Protection for Vaccines. (2022). New England Journal of Medicine 387, 2203–2206.
- Gilbert, P. B., Montefiori, D. C., McDermott, A. B., Fong, Y., Benkeser, D., Deng, W., et al. (2022). Immune correlates analysis of the mRNA-1273 COVID-19 vaccine efficacy clinical trial. *Science* 375, 43–50.
- Haneuse, S. and Rotnitzky, A. (2013). Estimation of the effect of interventions that modify the received treatment. *Statistics in medicine* **32**, 5260–5277.
- Hejazi, N. S., van der Laan, M. J., Janes, H. E., Gilbert, P. B., and Benkeser, D. C. (2021). Efficient nonparametric inference on the effects of stochastic interventions under two-phase sampling, with applications to vaccine efficacy trials. *Biometrics* 77, 1241–1253.
- Huang, Y., Hejazi, N. S., Blette, B., Carpp, L. N., Benkeser, D., Montefiori, D. C., et al. (2023). Stochastic interventional vaccine efficacy and principal surrogate analyses of antibody markers as correlates of protection against symptomatic COVID-19 in the COVE mRNA-1273 Trial. Viruses 15, 2029.
- Kallus, N., Mao, X., and Uehara, M. (2022). Causal inference under unmeasured confounding with negative controls: A minimax learning approach. Preprint 2022, arXiv:2103.14029v4.
- Kress, R. (2010). Linear Integral Equations. 3rd edition. New York: Springer.
- Miao, W., Geng, Z., and Tchetgen Tchetgen, E. J. (2018). Identifying causal effects with proxy variables of an unmeasured confounder. *Biometrika* **105**, 987–993.
- Muandet, K., Mehrjou, A., Lee, S. K., and Raj, A. (2020). Dual instrumental variable regression. *Advances in Neural Information Processing Systems* **33**, 2710–2721.
- Plotkin, S.A. (2010). Correlates of protection induced by vaccination. *Clinical and vaccine immunology* 17, 1055–1065.
- Robins, J. (1986). A new approach to causal inference in mortality studies with a sustained

- exposure period—application to control of the healthy worker survivor effect. *Mathematical modelling* **7**, 1393–1512.
- Sadoff, J., Gray, G., Vandebosch, A., Cárdenas, V., Shukarev, G., Grinsztejn, B., et al. (2022). Final analysis of efficacy and safety of single-dose Ad26.COV2.S. New England Journal of Medicine 386, 847–860.
- Schölkopf, B., Herbrich, R., Smola, A. J. (2001). A generalized representer theorem. In International conference on computational learning theory. Berlin, Heidelberg: Springer Berlin Heidelberg, pp. 416–426.
- Sholukh, A. M., Fiore-Gartland, A., Ford, E. S., Hou, Y. J., Tse, V., Kaiser, H., et al. Evaluation of SARS-CoV-2 neutralization assays for antibody monitoring in natural infection and vaccine trials. Preprint 2020, medRxiv: 2020-12.
- Shi, X., Miao, W., Nelson, J. C., and Tchetgen Tchetgen, E. J. (2023). Multiply robust causal inference with double-negative control adjustment for categorical unmeasured confounding. *Journal of the Royal Statistical Society Series B: Statistical Methodology* 82, 521–540.
- Tchetgen Tchetgen, E., Ying, A., Cui, Y., Shi, X., and Miao, W. (2020). An Introduction to Proximal Causal Learning. Preprint 2020, arXiv:2009.10982v1.

### SUPPORTING INFORMATION

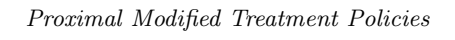
Web Appendix A, referenced in Section ??, is available with this paper at the Biometrics website on Wiley Online Library.

Received October 2007. Revised February 2008. Accepted March 2008.

## Appendix

## Title of appendix

Put your short appendix here. Remember, longer appendices are possible when presented as Supplementary Web Material. Please review and follow the journal policy for this material, available under Instructions for Authors at http://www.biometrics.tibs.org.



31

**Figure 1.** A causal directed acyclic graph of proximal causal inference. X and Y represent the exposure and outcome of interest; L and U the observed and unobserved confounders; and Z and W the negative control treatments and negative control outcomes, respectively.

Figure 2. (Panel A) Boxplots of the estimators and (Panel B) coverage probabilities for numerical experiments with data generated under varying conditional correlations of the proxies Z and W with the unmeasured confounder U and samples sizes n=750,1500,3000. In panel A, the dashed line indicates the true parameter value, while in panel B, it represents the nominal coverage level of 0.95. Non-proximal estimators are based on the assumption of no unmeasured confounding.

**Figure 3.** (Panel A) Observed and counterfactual probabilities of symptomatic COVID-19 infection and (Panel B) observed and counterfactual vaccine efficacy (VE) against symptomatic COVID-19 infection for policies that shift everyone's observed antibody levels by 0 (no shift), 0.2, 0.4, 0.6, 0.8, and 1 logarithm. The bars indicate the 95% confidence interval at each shift without any correction.